

Effects of Electrostatic Charge on Particle Adhesion, Powder Cohesiveness and its Alternative Influences on Powder Flow Properties

Tong Deng*, Vivek Garg, and Michael SA Bradley

Wolfson Centre for Bulk Solids Handling Technology, Faculty of Engineering & Science, University of Greenwich, Central Avenue, Chatham ME4 4TB, UK

Characterising powder flowability for handling process is important but can be particularly challenging if only a small quantity of samples is available. A novel method developed at the Wolfson Centre uses only a few milligrams of samples to predict powder flow properties by Bond number — a representation of powder cohesiveness at the median size of particles by measuring particle adhesion. A good agreement between this method and the results using conventional shear cell testers has been found across various powders and formulations. However, recent investigations on acetaminophens revealed a discrepancy: predictions based on the Bond number did not align with the shear cell test results, suggesting the presence of additional contributing forces during the Bond number measurement.

As the Bond number is determined by assessing particle adhesion, it was hypothesised that electrostatic forces could influence the adhesion results and therefore the Bond number. This study focused on the electrostatic charge measurements of two grades of acetaminophen (dense and micronised) with differing particle sizes. For a comparison, common excipients such as lactose, magnesium stearate, and calcium carbonate were also evaluated, all of which previously exhibited good predictive correlations. Results show that acetaminophen samples exhibited charge levels up to 20 times higher than the excipient materials. It is inferred that electrostatic forces can strongly influence particle adhesion, if charge is significant, though their effect appears negligible in shear cell testing. The study concludes that electrostatic forces can significantly contribute to particle adhesion and impact powder flow behaviour particularly at low consolidation stresses.

Keywords: Electrostatic force; Particle adhesion; Powder cohesiveness; Powder flow; Low consolidation stress; Mechanical Surface Energy Tester.

1 Introduction

Powder flow properties are critical in the design of bulk solids handling processes and must be characterised during formulation development prior to the process, particularly for pharmaceutical manufacturing. However, characterising flowability can be challenging when only a small quantity of sample is available at the early stage of formulation selection. Conventional methods of characterising powder flow properties, such as shear cell testing (Krantz et al., 2009), typically require tens to hundreds of grams of samples for a single test. Even newer devices like the SSSpinTester-X Powder Strength Tester (Johanson, 2012) still require around 0.5 cc of samples, which is about 1 gram, depending on the bulk density.

Sometimes the sample quantity could be very small, maybe only in grams especially for the active pharmaceutical ingredients (APIs). To confront this limitation of the small quantity of sample, a novel method was developed at the Wolfson Centre for predicting powder flow

* Email: t.deng@gre.ac.uk; Tel: +442083319951

41 properties only with a few milligrams of powders (Garg et al., 2022). This method employs a
42 Bond number representing powder cohesiveness in combination with physical properties
43 such as particle size and density to predict flowability of the powders. The Bond number is
44 determined by measuring particle adhesion at the median particle size using a mechanical
45 surface energy tester (Deng et al., 2021). Previous studies showed good agreement with
46 conventional methods such as shear cell tests across a wide range of powders differing in
47 particle size, shape, and density, suggesting the robustness of the approach (Deng et al., 2022).
48 However, recent works with different grades of acetaminophen revealed discrepancies: the
49 powder flow properties predicted using the Bond number did not align with the results
50 obtained from shear cell tests (Particle Flow Tester, Brookfield, USA). This indicated that there
51 might be additional contribution force contributing to the adhesion measurements made with
52 the mechanical surface energy tester.

53 In the determination of Bond number, which is defined as the ratio of particle adhesion force
54 to gravitational force, the particle adhesion is measured directly from the detachment of a
55 particle or numbers of particles on a flat substrate surface and then the Bond number is
56 calculated from the deceleration relative to gravitational acceleration. For particle adhesion,
57 there are three major contributions; Van der Waals forces, electrostatic forces, and capillary
58 forces (Salazar-Banda et al., 2007). Given the experimental conditions, electrostatic force was
59 suspected as the major cause of the discrepancies in the acetaminophen results.

60 The current study focused on measuring the electrostatic charge levels of two types of
61 acetaminophens (dense and micronised) with different particle sizes. For comparison,
62 common materials such as lactose, magnesium stearate, and calcium carbonate — which
63 previously showed good predictive correlation using the Bond number — were also evaluated.
64 Results of charge measurements demonstrated both dense and micronised acetaminophen
65 carried significantly higher electrostatic charges under normal handling conditions compared
66 to the other materials. A comparison of powder flow predictions with experimental results
67 suggests that electrostatic forces can strongly influence particle adhesion measurements and
68 affect powder flow properties at low consolidation stresses. However, their influence appears
69 negligible in shear cell tests, where higher consolidation stresses are typically applied.

70 Therefore, understanding the particle adhesion and its impact on powder flowability are
71 essential to interpret these findings. In particular, distinguishing the contributions of Van der
72 Waals forces, electrostatic forces, and capillary forces provides insight into the reliability and
73 limitations of Bond number-based predictions. This paper discusses the fundamental aspects
74 of particle adhesion, the key forces involved, and how these interactions influence powder
75 flow behaviour, especially under varying consolidation conditions.

76 2 Particle adhesion and influences on powder flow

77 2.1 Powder flow and influential factors

78 Flow properties of powders in processes are complex and primarily influenced by particle
79 size, shape, density, and internal friction (Shah et al, 2017). The flow properties of a powder
80 are commonly characterised by a number of parameters such as the angle of repose (AoR),
81 Hausner ratio (HR), and flow functions at different consolidation stresses (Baesso et al., 2021).
82 When powders exhibit similar physical properties, their flow behaviour is predominantly

83 determined by internal friction, which is itself affected by particle adhesion or cohesiveness
84 of the powder. Characterising these properties typically requires a significant quantity of
85 sample material for reliable measurement (Krantz et al., 2009).

86 For example, the angle of repose (AoR) is a widely used indicator of powder flowability,
87 reflecting the influence of particle size, shape, and cohesiveness, which is defined as the angle
88 between the free surface of a bulk solid pile and the horizontal plane. It. Since no external
89 consolidation stress is applied during the measurement, it is unlikely to be affected by powder
90 compaction. According to the Carr classification of flowability (ASTM D6393, 2009), the AoR
91 provides an indication of powder cohesiveness. However, for highly cohesive materials,
92 obtaining an accurate AoR is challenging. Al-Hashemi et al. (Al-Hashemi and Al-Amoudi, 2018)
93 concluded that the AoR does not directly correspond to either the peak or residual internal
94 friction angle as measured in direct shear tests. Furthermore, minor variations in sample
95 preparation or measurement technique can lead to significant errors, making AoR
96 measurements unreliable for the design of processing equipment such as silos and hoppers.
97 The AoR is also known to correlate well with the Hausner Ratio (HR) (Geldart et al., 2006),
98 which is defined as the ratio of a powder's tapped bulk density to its loose bulk density. Like
99 the AoR, the HR serves as a simple indicator of powder flowability. However, using HR for
100 practical equipment design faces similar challenges to the AoR due to its sensitivity to sample
101 handling and measurement conditions.

102 A more robust parameter for assessing powder flow is the Flow Function (FF), introduced
103 by Jenike (Jenike, 1967). The flow function characterises powder behaviour under compaction
104 and shear conditions by relating the major principal consolidation stress to the unconfined
105 yield strength, as shown in Eq. (1):

$$106 \quad \text{Flow Function } (ff) = \frac{\text{major principal stress, } \sigma_1}{\text{unconfined yield strength, } \sigma_c} \quad (1)$$

107 Flow function measurements involve determining the shear strength of a compacted
108 powder bed under controlled consolidation loads. A review (Al-Hashemi and Al-Amoudi, 2018)
109 summarised that the key factors influencing powder flow include particle properties (size,
110 shape, density), cohesive forces (e.g., Van der Waals forces, electrostatic interactions,
111 capillary bridging), and compaction effects (determined by particle contact points and packing
112 density). These complex interactions, especially under combined compaction and shear
113 conditions, require extensive testing and repeated measurements to ensure accuracy (Peleg
114 et al., 1973).

115 Compared to AoR and HR, the flow function provides a more representative basis for
116 designing material handling equipment. However, a significant limitation of common flow
117 function testing is the quantity of sample required, often tens of grams per test. While this is
118 manageable when large quantities of powder are available, it poses a major challenge when
119 sample availability is limited to less than a gram, such as early formulation development
120 stages for pharmaceuticals (Cun et al., 2021).

121 2.2 Prediction of powder flow with a small quantity of samples

122 A prediction method of powder flow using a small quantity of samples was developed
123 based on correlations between powder flowability and cohesiveness of powders, where a

124 Bond number was used for representing powder cohesiveness (Garg et al., 2022). A linear
 125 relationship between Bond numbers (Bo) and flow functions under different consolidation
 126 stresses was used to predict powder flow based on an intuitive assumption that ‘highly
 127 cohesive powder is more difficult to flow’ (Deng et al., 2022). The prediction model is
 128 expressed in Eq. 2, in which the gradient and the intercept of the linear relationship are shown
 129 in Eq. 3 and Eq. 4 as a function of consolidation stress levels (σ_1).

$$130 \quad 1/ffc = m(Bo) + c \quad (2)$$

$$131 \quad \text{where} \quad m = a_1 \ln(\sigma_1) + b_1 \quad (3)$$

$$132 \quad c = a_2(\sigma_1)^{b_2} \quad (4)$$

133 where a_1 , a_2 , b_1 and b_2 are constants. If they are taken as -0.020, -0.442, 0.117 and -0.073,
 134 respectively, from a previous study (Garg et al., 2022; Deng et al., 2022), the prediction model
 135 can be:

$$136 \quad 1/ffc = [-0.020 \ln(\sigma_1) + 0.117](Bo) - 0.442(\sigma_1)^{-0.073} \quad (5)$$

137 In this method, powder flow properties are correlated to the physical properties of the
 138 particles, their cohesiveness, and compaction characteristics through the Bond number and
 139 consolidation stress (σ_1). Comparative studies have demonstrated successful predictions for
 140 various powder types, including mixtures of different formulations (Deng et al., 2022). This
 141 method offers significant advantages for determining powder flow properties using
 142 milligrams of sample material, especially when only limited sample quantities are available
 143 during the formulation development stage or pre-manufacturing process design for large-
 144 scale production.

145 2.3 Particle adhesion and Bond number

146 In the prediction model (using milligrams of sample), the Bond number is a key parameter
 147 representing powder cohesiveness at the particle size of D_{50} (Deng et al., 2021). The Bond
 148 number (Bo) is defined as a ratio of particle adhesion force, F_{ad} , to the gravity force of the
 149 particle, F_g , for cohesive particles, as shown in Eq. 6.

$$150 \quad Bo = F_{ad}/F_g = F_{ad}/(mg) \quad (6)$$

151 where the particle adhesion (F_{ad}) of particles is measured using a mechanical surface energy
 152 tester (Deng et al., 2021), which requires only milligrams of sample material containing a
 153 sufficient number of particles (typically hundreds, depending on the particle density).

154 It is important to note that the particle adhesion measured in this method has a significant
 155 impact on the results (Deng et al., 2021). The adhesion force between particles or between a
 156 particle and a surface consists of three primary components: Van der Waals forces,
 157 electrostatic forces, and capillary forces, as shown in Eq. (7) (Salazar-Banda et al., 2007). The
 158 relative magnitude of each force depends on the physicochemical properties of the materials
 159 in contact, as well as the contact orientation and the separation distance between particles
 160 or the particle and the surface (Quintanilla et al., 2006).

$$161 \quad F_{ad} = F_{vw} + F_e + F_{cf} \quad (7)$$

162 where F_{vw} is Van der Waals force, F_e is electrostatic force, and F_{cf} is capillary force.
 163 Characterising each individual force can be challenging; however, theoretical estimations for
 164 each force have been proposed in the literature, typically based on the assumption of
 165 perfectly rigid particles in contact, such as spherical particles (Mittal and Jaiswal, 2015; Tomas,
 166 2000). These theories often assume specific separation distances between particles and their
 167 influence on particle adhesion measurements, but this remains an area of ongoing debate
 168 (Mullins et al., 1992). In this study, the focus is placed on the contribution of electrostatic
 169 force to particle adhesion, an effect that has been recognised for many years (Donald, 1969),
 170 yet is still not fully understood. Sometimes, the charge influence can be obvious.

171 3 Materials and methods

172 3.1 Test Materials

173 The powder samples used in this study included acetaminophen dense and acetaminophen
 174 micronised, which are known for their high chargeability. For comparison, three commonly
 175 used powders were selected: Calcium Carbonate, Lactose, and Magnesium Stearate. These
 176 materials have shown good agreement with the prediction model previously established. The
 177 characteristics of the materials, including particle size, size span, particle solid density, and
 178 Bond numbers (measured using a mechanical surface energy tester (Deng et al., 2021)), are
 179 provided in Table 1, which is described in the following section.

180 **Table 1: MATERIALS STUDIED AND MATERIAL PHYSICAL PROPERTIES**

Materials	Particle Size (μm)			Size Span ($(D_{90}-D_{10})/D_{50}$)	Solid Density (kg/m^3)	Bo Number
	D_{10}	D_{50}	D_{90}			
Acetaminophen dense	16	63	207	3.03	1356 ± 20	8.9 ± 0.2
Acetaminophen micronised	2	6	19	1.78	1380 ± 10	9.1 ± 0.1
Eskal 4 (Calcium Carbonate)	2	4	13	2.76	2800 ± 30	8.6 ± 0.2
Granulac 70 (Lactose)	19	90	118	1.10	1560 ± 50	8.2 ± 0.3
Magnesium Stearate	1.5	6.0	18.4	2.80	1600 ± 25	7.8 ± 0.2

181 3.2 Experimental methods

182 3.2.1 Particle size and density measurements

183 The particle sizes of the powders were measured using laser diffraction (Mastersizer 3000,
 184 Malvern Panalytical Ltd, UK) with a dry feeding method. For each sample, approximately 7g
 185 of powder was used, and five repeat measurements were conducted at 2 bar air pressure and
 186 a 50% feed rate. The average result of all measurements was used for the predictions.

187 The size span (S_{span}) was calculated using Eq. (8) by the size distributions measured,
 188 representing the particle size range that significantly influences powder flow behaviour:

$$189 \quad S_{\text{span}} = (D_{90} - D_{10})/D_{50} \quad (8)$$

190 where D_{50} represents the size in diameter, where the percentage of powder is less or equal
 191 to 50% in volume. D_{10} and D_{90} are the sizes where 10% and 90% of the powder is below the
 192 size, respectively.

193 Particle density was measured using a gas pycnometer (Ultracyc 1200e, Quantachrome
194 Instruments, USA), employing nitrogen gas. Five repeated measurements were taken, with
195 the standard deviation being approximately 0.05% of the mean value. The solid density was
196 used for the predictions of powder flow properties.

197 3.2.2 Mechanical surface energy tester

198 A mechanical surface energy tester developed at the Wolfson Centre was used to measure
199 particle adhesion and Bond number (Bo) (Deng et al., 2021). Approximately 50 mg or less of
200 sample powder was deposited on a 40 mm diameter glass substrate using an air expansion
201 disperser at 1.5 bar pressure. After deposition, the mass of the sample was measured using a
202 digital balance (accuracy: 0.1 mg). The sampled substrate was discharged under gravity
203 through a guide rod at a certain height, where the particles decelerated upon hitting a metal
204 buffer. The acceleration generated during the impact was recorded for Bo measurements.

205 The mass of the detached particles was measured by measuring the substrate again. The
206 detached particles collected were then analysed under a Malvern G3 microscope (Malvern
207 Panalytical Ltd, UK) to determine the median particle size (D_{50}) and to examine the number
208 and nature of the detached particles. The Bond number (Bo) was calculated using the
209 deceleration value and adhesion force, as shown in Eq. (6).

210 3.2.3 Powder flow properties and shear tester

211 The powder flow properties were measured using a shear cell powder flow tester (PFT)
212 (Brookfield Engineering Laboratories Inc., Middleboro, MA, USA), which is typically used for
213 determining flow functions under consolidation stresses (Garg et al., 2018). The PFT consists
214 of an annular shear cell (263 cm³ for the standard cell, or 43 cm³ for a small cell). Powder
215 sample was loaded into the cell evenly, and the sample weight was measured using a digital
216 balance (accuracy: 1 mg) before undertaking the measurement.

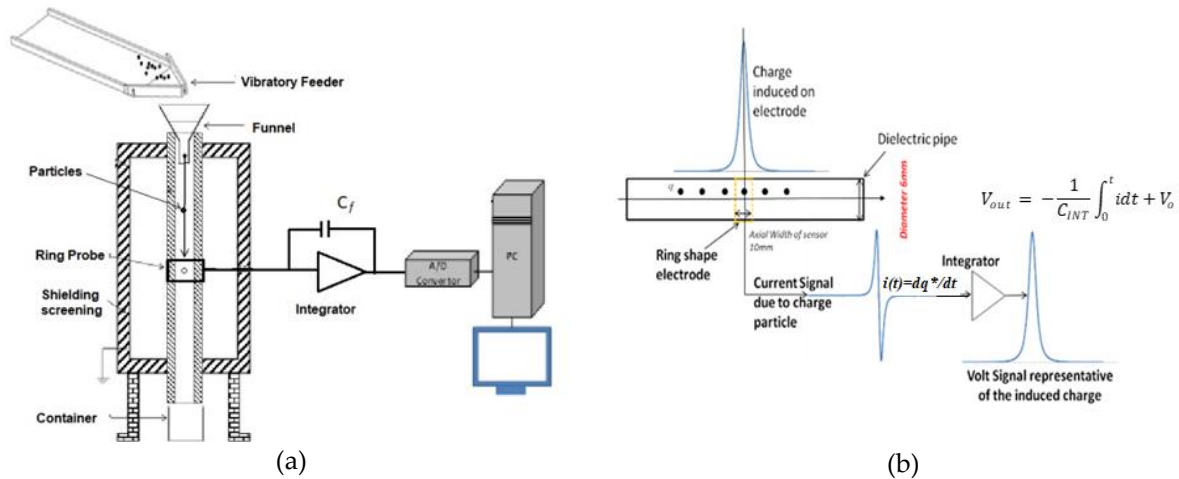
217 During testing, a top-knifed lid was applied to the powder bed, and a series of consolidation
218 stresses were sequentially applied. Once a desired consolidation stress level was achieved,
219 shear forces were then applied to the cell, compacting the powder. The torque generated
220 through the powder bed to the lid was recorded and used to calculate the Mohr's circle and
221 the unconfined yield strength at each consolidation stress level. The tests were conducted at
222 ambient temperature (about 20-25°C and 40-60% RH), using Powder Flow Pro software to
223 generate yield locus and flow functions as a function of major principal consolidation stress.

224 3.2.4 Electrostatic charge and inductive charge sensor

225 An inductive charge sensor previously developed at the Wolfson Centre was used to detect
226 triboelectric charging accumulation over a number of particles (Hussain et al., 2013). The
227 sensor, shown in Fig. 1a, consists of an inductive sensor ring, a pure integrator, and signal
228 data acquisition. The charged particles passing through the sensor ring generate an image
229 charge on the sensor, which produces a current signal that is integrated into a voltage signal
230 for charge detection of a single particle or a cluster of particles (see Fig. 1b). The charge tests
231 were conducted also at ambient temperature (~20°C) and humidity (40-50% RH).

232 The sensor setup also includes a particle delivery tube (200 mm long, 6 mm in diameter)
233 and a shielding screening box. When a particle with charge $\pm q$ passes through the sensor, the

234 induced voltage pulse magnitude is proportional to the charge divided by the capacitance of
 235 the feedback capacitor (10 pF). The total charge accumulated over all particles passing
 236 through the sensor is used to calculate the charge level of the powders. The total mass of the
 237 particles was also measured after collection using a digital balance (accuracy: 0.1 mg),
 238 allowing for the calculation of the charge level per unit mass of powder.



239 **Figure 1:** Inductive charge sensor: (a) Schematic of the inductive charge sensor with a pure
 240 integrator, (b) principle of the inductive charge sensor (Deng et al., 2023).

241 4 Results and discussion

242 4.1 Flow properties

243 The flow properties of the powders used for this study are measured, including angle of
 244 repose (AoR), Hausner Ratio (HR), compression index (CI), and flow function coefficients (FFc)
 245 at five different major principal consolidation stresses by a PFT shear tester. The AoR was
 246 measured using the lifting column method. The Hausner Ratio (HR) and the compression
 247 index were measured using pore bulk density and tapped bulk density with 1050 taps applied.
 248 Characteristics of the flow properties of the materials studied are given in Table 2. The flow
 249 functions measured using PFT are compared with the predictions using the model with the
 250 Bond number measured.

251 **Table 2: Flow properties measured of the powder materials**

Materials	AoR (°)	HR	CI	FFc (0.8 kPa)	FFc (1.25 kPa)	FFc (2.25 kPa)	FFc (4.8 kPa)	FFc (9.0 kPa)
Acetaminophen dense	52	1.56	36	1.810	1.827	1.724	2.226	3.774
Acetaminophen micronised	55	1.59	38	1.653	1.669	1.669	2.045	3.513
Eskal 4 (Calcium Carbonate)	49	1.52	33	1.178	1.021	1.046	1.663	2.442
Granulac 70 (Lactose)	46	1.44	31	1.942	1.025	1.052	1.425	2.188
Magnesium Stearate	60	1.62	40	1.070	1.006	1.018	1.242	1.792

252 The particle adhesion forces measured using the mechanical surface energy tester are
 253 presented in Table 3, which also includes the mass of particles before and after the tests. The
 254 calculated Bo numbers are also presented in the table here represent each corresponding
 255 sample materials tested in this study. The predicted flowabilities of the sample powders
 256 derived using the Bo number and the model shown in Eq. 5 are given in Table 3.

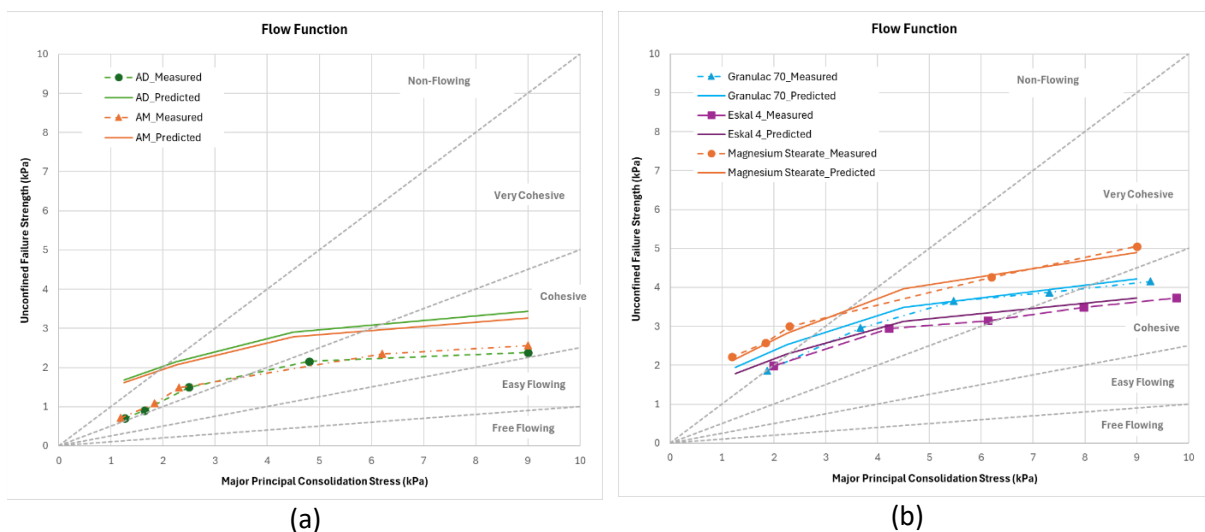
257 **Table 3: Particle adhesion measured, Bo number and the flow functions predicted**

Materials	F_{ad} ($\times 10^{-5}$ N)	Mass (before) (mg)	Mass (after) (mg)	Bo Num.	FFc (0.8 kPa)	FFc (1.25 kPa)	FFc (2.25 kPa)	FFc (4.8 kPa)	FFc (9.0 kPa)
Acetaminophen dense	9.909	2.08	1.28	8.9 ± 0.2	1.81 0	1.82 7	1.72 4	2.226	3.774
Acetaminophen micronised	8.782	2.08	1.03	9.1 ± 0.1	1.65 3	1.66 9	1.66 9	2.045	3.513
Eskal 4 (Cal. Carbonate)	9.831	2.08	1.32	8.6 ± 0.2	1.17 8	1.02 1	1.04 6	1.663	2.442
Granulac 70 (Lactose)	9.314	2.08	1.32	8.2 ± 0.3	1.94 2	1.02 5	1.05 2	1.425	2.188
Magnesium Stearate	9.796	2.08	1.47	7.8 ± 0.2	1.07 0	1.00 6	1.01 8	1.242	1.792

258

259 4.2 Comparison between the measured and the predicted flow functions

260 The predicted flow functions of the sample powders were compared with the measured
 261 flow functions using the PFT shear tester, as shown in Fig. 2. In Fig. 2a, the acetaminophen
 262 results exhibit a significant disparity between the predicted and measured flow functions. The
 263 differences between the predictions and the measurements clearly identify that there are
 264 some factors that influence the measurement of particle adhesion, which could be significant
 265 in the adhesion measurement but insignificant in the bulk powder flow measurements. As
 266 shown in Fig. 2b, the prediction for the other common materials (Granulac 70, Eskal 4 and
 267 Magnesium Stearate) shows a good agreement with the experimental results.



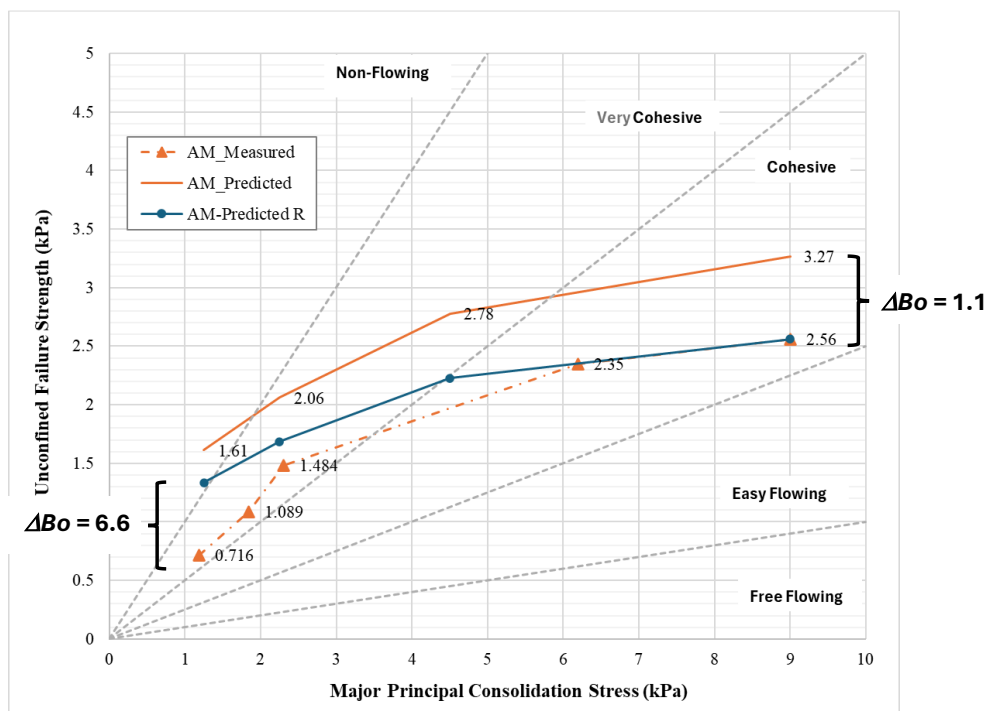
268 **Figure 2: Instantaneous flow functions measured and predicted of: (a) Acetaminophen**
 269 **dense and micronised, (b) Lactose, Calcium Carbonate, and Magnesium Stearate.**

270 4.3 The differences in predicted flow functions

271 The results in Fig. 2a demonstrate that the predicted flow function for both acetaminophen
 272 dense and micronised is significantly higher than that measured using a PFT shear tester. It is
 273 also noted that for the acetaminophen the prediction at low consolidation stress is much
 274 higher than that measured using a PFT, but at the high consolidation stress, the difference
 275 between the predicted and the measured flow functions is decreasing when the consolidation
 276 stress is over 4.8 kPa (see Fig. 3).

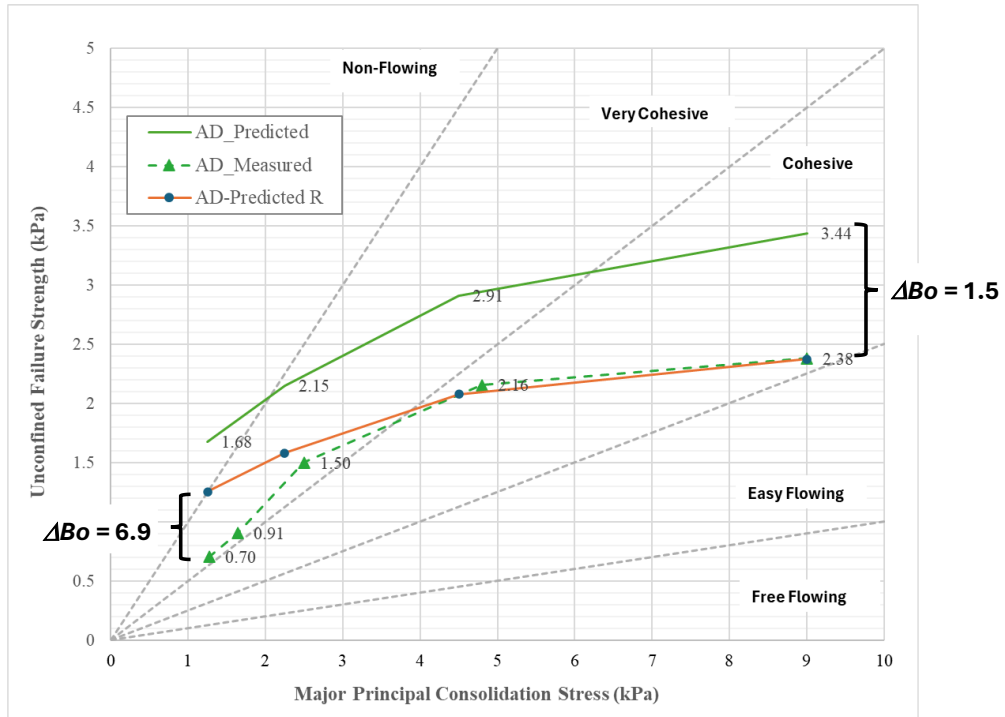
277 In comparison, the flow functions for three other materials were predicted using the same
 278 method and compared to the measurements using a PFT. The comparison between Fig. 1a
 279 and 1b indicates there must be an influence on the particle adhesion measurement, which
 280 would give a quite different predictions on powder flow properties. With the influential
 281 factors considered for particle adhesion, except the capillary force, the electrostatic force is
 282 thought most likely to be significant, as shown in Eq. 7.

283 In the powder flow properties, powder cohesiveness contributes to the internal friction
 284 force between the particles. At high consolidation stress, the distance between particles can
 285 be reduced due to compaction. The increase in internal frictional force may be due to the
 286 increased contact areas between the particles. At the low consolidation stress, because of
 287 increased distances and decreased contact areas between the particles, particle adhesion can
 288 become a main donor influencing powder cohesiveness. Using the Bond number to represent
 289 the particle cohesiveness for the prediction of powder flow, the results in Fig.1a show the
 290 differences. Taking the differences for estimating the defences in Bond numbers, the Bo
 291 difference can be used for estimating the difference in particle adhesion measurements (see
 292 Fig. 3).



293

(a)



(b)

294

295 **Figure 3:** The difference between the predicted flow function and the measured result and
 296 indication of the Bo number difference (a) acetaminophen micronised, (b) acetaminophen
 297 dense.

298 4.4 Charge levels of the powders

299 The difference in the predicted flow functions for acetaminophen, as determined by the
 300 Bond number, indicates that particle adhesion measurements are influenced by additional
 301 factors. Electrostatic charge is identified as the primary factor contributing to the observed
 302 differences in powder cohesiveness, as it affects the levels of particle adhesion detected. To
 303 assess the electrostatic influence on the powder flow properties, the charge levels and
 304 polarity distributions of the sample powders were measured using an inductive charge sensor
 305 developed at the Wolfson Centre.

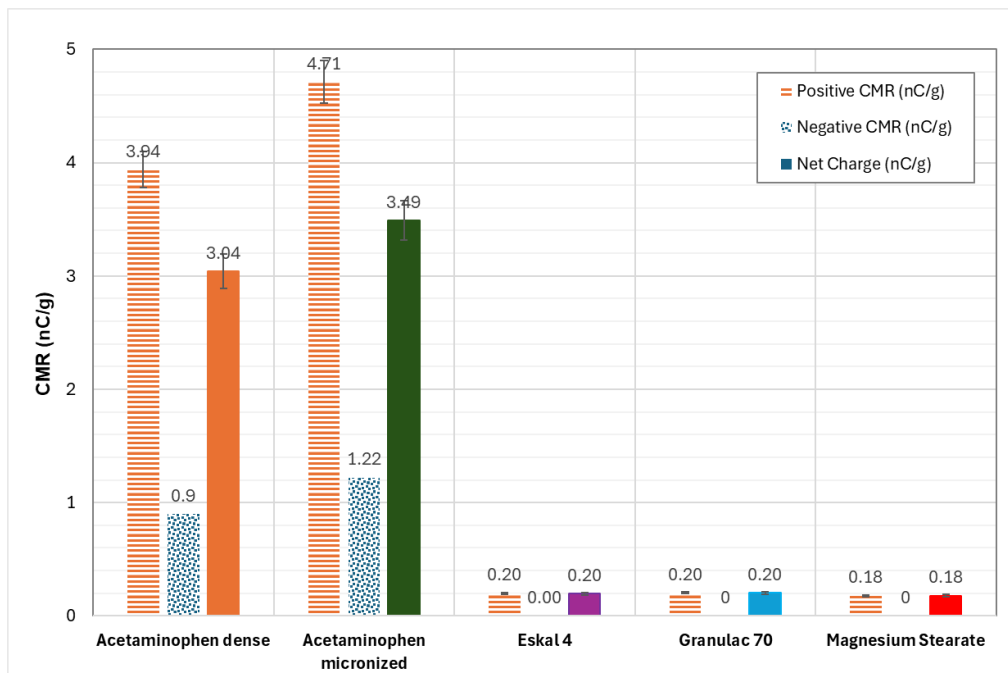
306 For this study, the charge-to-mass ratio (CMR) was employed as a measure of the particle
 307 "chargeability," which quantifies the charge level relative to the mass of the sample. The CMR
 308 is defined and expressed in Eq. 9 as follows:

309
$$CMR = \frac{Q}{m} = \frac{\Delta V_o \cdot C_f}{m}, \quad (9)$$

310 where, CMR is the charge-to-mass ratio (C/kg, Coulomb per kilogram), m is the mass of the
 311 test sample (kg), ΔV_o is the output voltage (V) measured by the sensor, and C_f is the feedback
 312 capacitor (F) of the virtual earth amplifier used by the sensor. In the study, nC/g is used for
 313 the results, which is equal to 10^{-9} C/kg. Positive values of CMR express the positive charge of
 314 powders and negative values of CMR mean a level of negative charge. The net charge level is
 315 the sum of the positive charge and the negative change measured in the same tests. The
 316 results for all comparative materials are shown in Fig. 4. Acetaminophen micronised exhibits
 317 the highest net charge level of 3.49 nC/g, while acetaminophen dense has a net charge level

318 of 3.04 nC/g. In comparison to the other powders—Calcium Carbonate, Lactose, and
 319 Magnesium Stearate—the charge levels of acetaminophen are approximately 20 times higher
 320 at the maximum and 15 times higher at the minimum. These charge levels were observed in
 321 a natural environment, without any external triboelectric charging actions, suggesting
 322 intrinsic charge differences among the materials.

323 Furthermore, both acetaminophen-dense and micronised powders exhibit bipolar charge
 324 distributions, whereas the other powders are unipolar. This difference indicates that the
 325 contribution of static charge to powder cohesiveness is much higher for acetaminophens
 326 compared to the common materials tested. The enhanced static charge in acetaminophen
 327 plays a major role in its powder cohesiveness and contributes to the observed deviations in
 328 flow function predictions, particularly in powders with low consolidation stress.



329 **Figure 4:** Overall charge-to-mass ratios and polarity distributions for the acetaminophen
 330 powders and comparative materials.
 331

332 4.5 The static charge and influences

333 Previous studies (Suhag et al., 2024) have shown that multiple factors contribute intricately
 334 to powder flowability, including physical properties such as particle size, shape, density, and
 335 cohesiveness. The cohesiveness of powders is contributed to collectively by solid particles,
 336 moisture content, and other internal forces such as electrostatic force.

337 The flow behaviour of powders becomes increasingly complex when subjected to
 338 compaction stress, as variations in powder cohesiveness can arise due to environmental
 339 influences or the specific test conditions and methods applied. While the influence of
 340 electrostatic forces on powder flow properties is often overlooked in evaluations of powder
 341 flow, it is a common phenomenon in manufacturing processes. Despite its relevance, the role
 342 of electrostatic charging in powder flow properties has been insufficiently studied (Rescaglio
 343 et al., 2017; Lefebvre et al., 2021), largely due to its perceived inefficiency. However, the

344 effects of electrostatic charge may become significant when powders are finer or when they
 345 flow under low consolidation stress (Liu et al., 2023; Karner et al., 2011).

346 By Coulomb's law, the magnitude of electrostatic force, F_e , between two-point charges, q_1
 347 and q_2 separated by a distance r , can be calculated using the following equation.

$$348 \quad F_e = k \frac{|q_1 \cdot q_2|}{r^2} \quad (10)$$

349 where in SI units, the constant k is equal to $8.988 \times 10^9 \text{ N} \cdot \text{m}^2 / \text{C}^2$. Coulomb's law provides the
 350 magnitude of the force between point charges, but it may not be entirely applicable to the
 351 case studied here. In the context of powder flow and particle adhesion, the electrostatic force
 352 between a charged particle and a surface is often estimated using the image force model
 353 (Mizes et al., 2000). In this model, the force exerted by the particle charge is attracted to its
 354 image charge in the substrate. The electrostatic force, in this case, is proportional to the
 355 square of the total charge, as represented by Eq. 11.

$$356 \quad F_e = a(\epsilon_p \& \text{sub}) \frac{Q^2}{16\pi\epsilon_0 R^2} \quad (11)$$

357 where Q is the net charge on the particle of radius R , and ϵ_0 is the permittivity of free space
 358 and is equal to $8.85 \times 10^{-12} \text{ C}^2 / \text{N} \cdot \text{m}^2$. The coefficient a depends on the dielectric constants of
 359 the particle and the substrate. For a uniformly charged sphere with a dielectric constant equal
 360 to 3 resting on a conductive substrate in the air ($\epsilon_{\text{substrate}} = \infty$), the constant a is about 1.59
 361 (Feng and Hays, 2003). However, this value of a is typically 5 to 50 times smaller than the
 362 corresponding measured value (Hays, 1995).

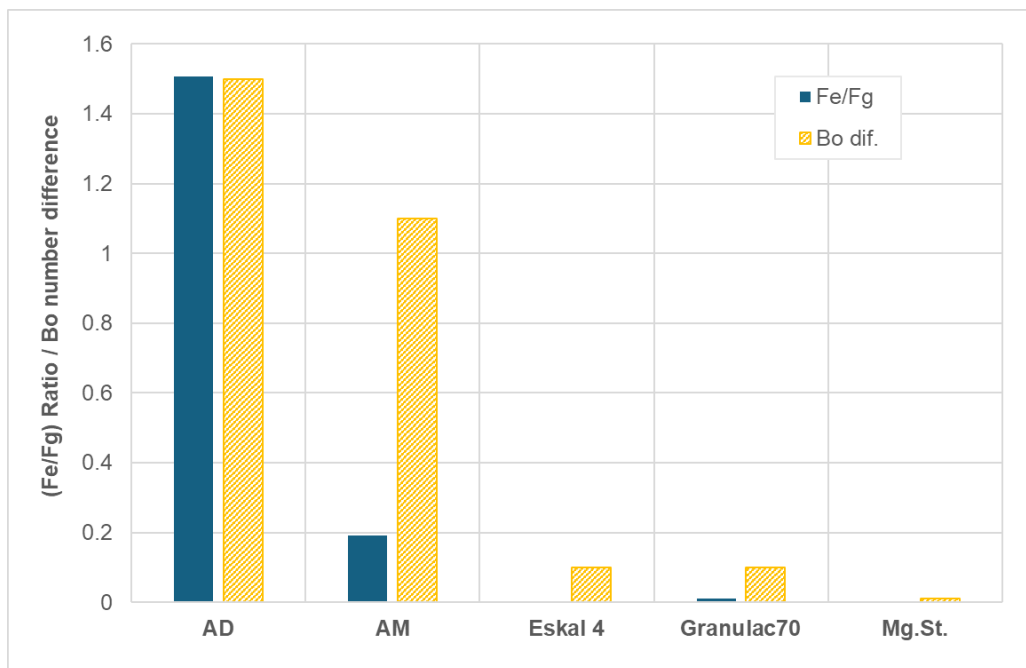
363 The results shown in Fig. 4 demonstrate that acetaminophen powders exhibit significantly
 364 higher chargeability compared to the other three materials, with net charge levels
 365 approximately 20 times greater than those of Calcium Carbonate, Lactose, and Magnesium
 366 Stearate. Using the charge levels measured in this study and referencing Zhou's study (Zhou
 367 et al., 2003), the electrostatic force can be estimated by applying Eq. 11. The results of this
 368 estimation are summarised in Table 4.

369 **Table 4: Electrostatic charge force calculated and the adhesion difference from the Bo**

Materials	D50 (μm)	Net Charge (nC/g)	F_e (N)	Volume (m^3)	F_g (N)	Bo	Bo dif.	F_e/F_g
Acetaminophen dense	63	3.04	$2.62 \cdot 10^{-9}$	$1.31 \cdot 10^{-13}$	$1.74 \cdot 10^{-09}$	8.9	1.5	1.506
Acetaminophen micronised	6	3.49	$2.95 \cdot 10^{-13}$	$1.13 \cdot 10^{-16}$	$1.53 \cdot 10^{-12}$	9.1	1.1	0.192
Eskal 4	4	0.20	$8.18 \cdot 10^{-16}$	$3.35 \cdot 10^{-17}$	$9.20 \cdot 10^{-13}$	8.6	0.1	0.001
Granulac 70	90	0.20	$6.26 \cdot 10^{-11}$	$3.81 \cdot 10^{-13}$	$5.84 \cdot 10^{-09}$	8.2	0.1	0.011
Magnesium Stearate	6	0.18	$1.19 \cdot 10^{-15}$	$1.13 \cdot 10^{-16}$	$1.88 \cdot 10^{-12}$	7.8	0.01	0.001

370 In Table 4, the Bo difference for acetaminophen dense was used to calibrate the
 371 electrostatic charge force calculation. Since the dielectric constant (a) is unknown, it was
 372 selected to match the ratio of charge force to gravity, as shown in the table. In this case, the

373 value of a was determined to be 1.59×2500 , which is approximately 2500 times higher than
 374 the theoretical value reported in the literature (Techaumnat and Takuma, 2009). Despite this
 375 discrepancy, applying the same value of a , the electrostatic charge forces for the other
 376 materials were calculated. These calculations reveal that the influence of electrostatic charge
 377 on acetaminophen micronised is substantial, while the effect on the other three materials is
 378 negligible. The comparison of charge force to gravity ratios and Bo number differences, as
 379 calculated from the shear test results and the predictions from the model, is shown in Fig. 5,
 380 clearly highlighting the impact of electrostatic charge force. A potential explanation for the
 381 2500 times higher value compared to theoretical estimates may lie in the presence of
 382 agglomerates. Unlike the theoretical model, which assumes a single particle, actual powder
 383 clusters can contain over 500 particles, which could account for the observed discrepancy.



384

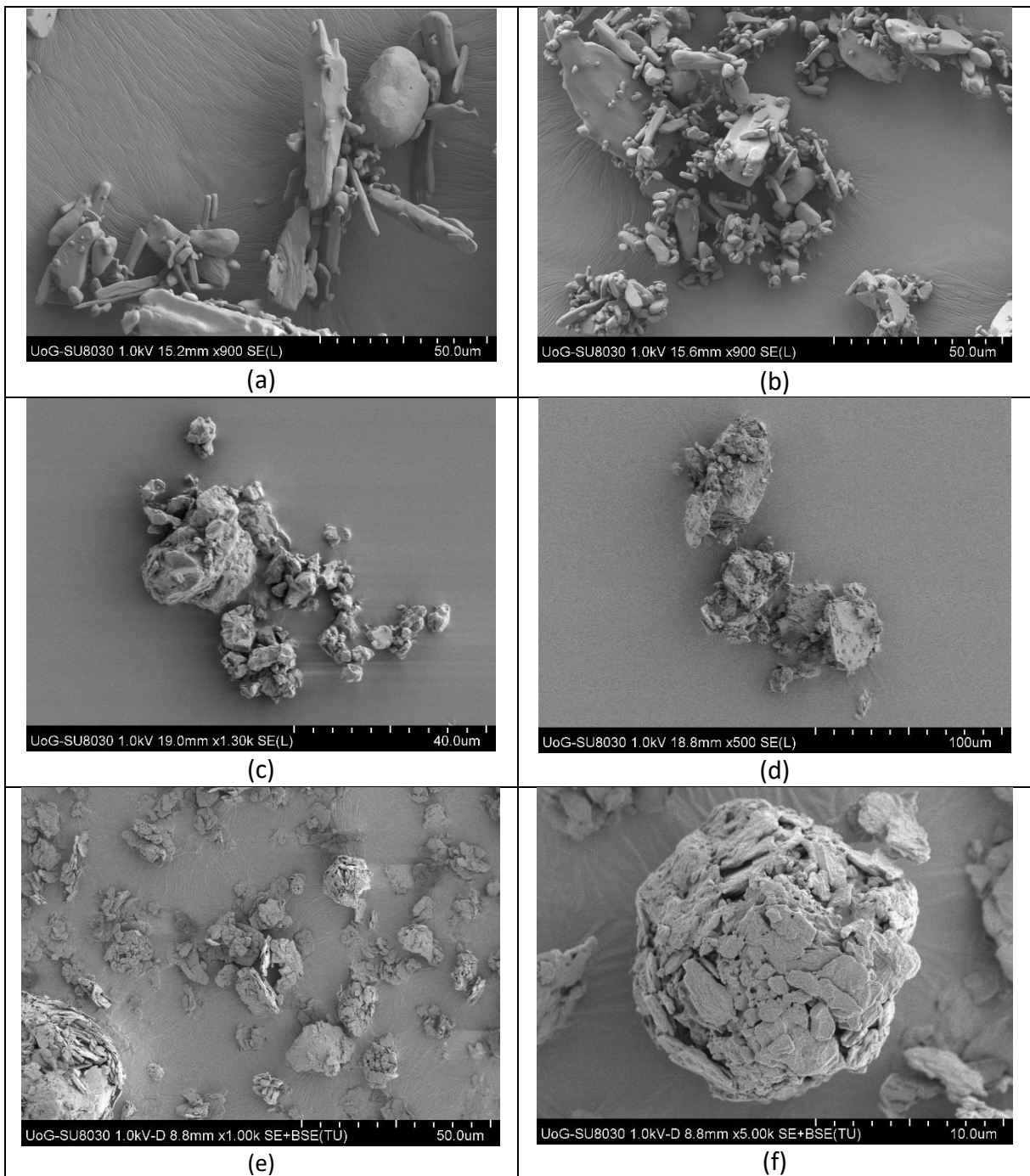
385 **Figure 5:** The comparison between the charge force to gravity ratios and the Bo number
 386 differences calculated from the shear test results and the prediction by the model.

387 4.6 Influences of static charge on powder flow

388 In both charge detection and Bo measurement, it is often challenging to detect individual
 389 particles due to significant agglomeration of particles, as observed with the acetaminophen
 390 samples shown in Fig. 6a and 6b. In both measurement techniques, the accuracy of results is
 391 highly dependent on the dispersion of the particles. During Bo detection, the gravity of the
 392 detached particles is measured based on their accumulated weight, while in charge detection,
 393 the detected charge level is typically based on agglomerates rather than individual particles
 394 as shown in Fig. 7. This leads to the possibility of significantly underestimating the true charge
 395 level, which could, in turn, affect the accuracy of adhesion measurements.

396 Fig. 7 illustrates a charge measurement for a 0.2 mg sample of powder, which is composed
 397 of four agglomerates. Each agglomerate weighs approximately 0.05 mg and contains about
 398 270 particles with an average size of 63 μm . When considering the agglomeration of the
 399 powders, this could help explain the observed 2500-fold increase in the dielectric constant,

400 as the theoretical model assumes the interaction of a single particle, while in reality,
401 agglomerates are involved. This indicates that charge effects on powder flow properties can
402 be significantly influenced by the extent of agglomeration, especially when it is substantial.

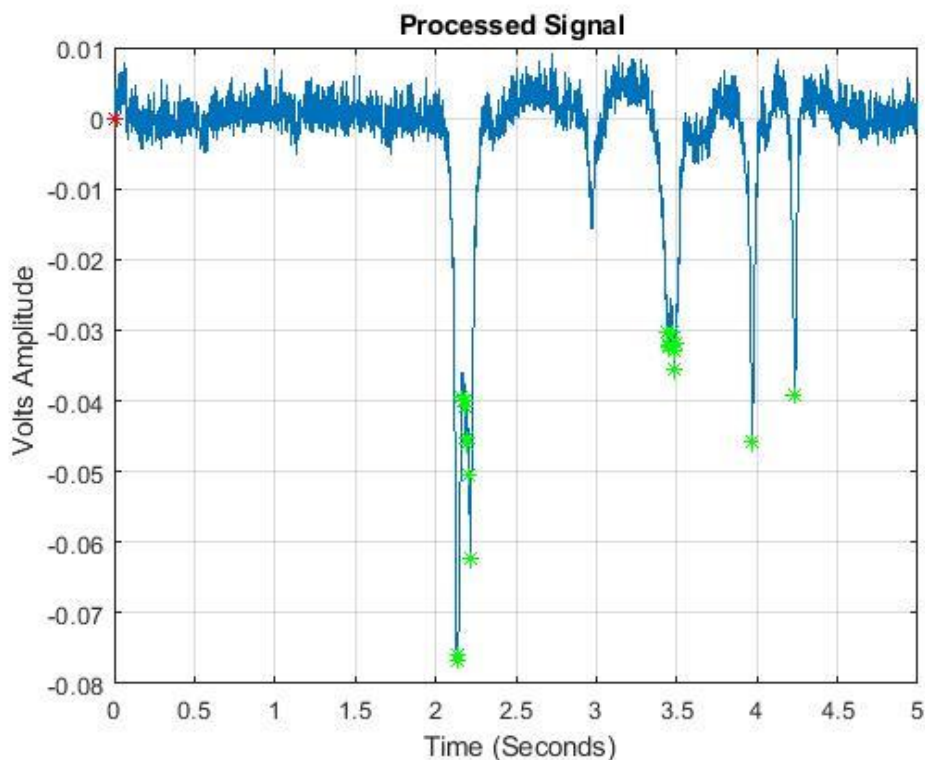


403 **Figure 6:** SEM images of the sample materials tested: (a) Acetaminophen dense, (b)
404 Acetaminophen micronised, (c) Eskal 4, (d) Granulac 70, and (e, f) Magnesium Stearate

405 The results in Fig. 3 demonstrate the influence of particle adhesion and agglomeration on
406 flow functions at low consolidation stress. In principle, cohesive materials tend to remain as
407 non-flowing powders, as observed for the three common materials tested here—Lactose,
408 Calcium Carbonate, and Magnesium Stearate. However, for acetaminophens, the measured
409 flow functions were much lower than those predicted by the model, suggesting the presence

410 of factors affecting particle adhesion that do not influence shear cell measurements. The most
411 suspicious candidate for this discrepancy is electrostatic charge, which is believed to be
412 expressed through agglomeration. As the consolidation stress increases, the influence of
413 charge diminishes, likely due to the reduction in the number of agglomerates, which
414 ultimately allows the flow properties to align more closely with model predictions.

415 Comparing the images shown in Fig. 6 may help to understand the influence of static
416 charging on the measurement of flow functions under consolidation stresses. For the low
417 chargeable materials such as Magnesium Stearate (see Fig. 6e and 6f), the agglomeration
418 seems denser than that highly chargeable materials such as acetaminophen micronised (see
419 Fig. 6b). The electrostatic charge on particles could make loose agglomerations compared to
420 uncharged materials. This influence on agglomeration will be compromised by consolidation
421 stress so the charge seems have a large effect on powder flow at low consolidation stress but
422 will not appear at the high consolidation stress.



423

424 **Figure 7:** A charge measurement of acetaminophen dense with a total sample mass of 0.2
425 mg (4 clusters accounted for the charge measurement) at the net charge level of -5.2nC/g.

426 5 Conclusions

427 This study has provided a comprehensive examination of the phenomena influencing
428 powder flow under varying consolidation stresses, highlighting the impact of factors such as
429 material properties, electrostatic charging, and more. While the prediction model based on
430 the Bond number (Bo) and particle size distributions has been validated through numerous
431 studies, it also presents certain limitations. Notably, the prediction model tends to
432 overestimate powder flow properties for acetaminophen, as compared to the results
433 obtained using shear cell testing.

434 The overestimation in acetaminophen predictions suggests that additional forces, likely
435 stemming from electrostatic charges, are contributing to an increased Bo number. A detailed
436 comparison of measured and predicted flow functions reveals that acetaminophen particles
437 exhibit charge levels significantly higher than those of the other materials studied, such as
438 Calcium Carbonate, Lactose, and Magnesium Stearate. Specifically, acetaminophen charge
439 levels were found to be approximately 20 times higher, as confirmed by measurements using
440 an inductive charge sensor.

441 It was found that the impact of static charge on acetaminophen-dense particles, when
442 calibrated, is approximately 20%, whereas the influence on Calcium Carbonate, Lactose, and
443 Magnesium Stearate is negligible, below 1%. Furthermore, SEM imaging of the powders
444 revealed that acetaminophen particles are highly agglomerated, which likely contributes to
445 discrepancies in charge detection. The agglomerates, often containing up to 270 particles, are
446 believed to influence the charge measurements.

447 The study concludes that electrostatic charge and particle agglomeration play significant
448 roles in powder cohesiveness, especially at low consolidation stresses. As consolidation stress
449 increases, the effects of charge and agglomeration on powder flow properties decrease,
450 aligning with observed practical behaviour. This study underscores the need for improved
451 models that account for these factors, particularly in the early stages of material development
452 when sample quantities may be limited.

453

454 References

- 455 Al-Hashemi, H. M. B., & Al-Amoudi, O. S. B. (2018). A review on the angle of repose of granular
456 materials. *Powder technology*, 330, 397-417.
- 457 ASTM D6393–08, 2009, "Standard Test Method for Bulk Solids Characterization by Carr Indices,"
458 Annual Book of ASTM Standards, Vol. 04.09, ASTM International, West Conshohocken, PA.
- 459 Baesso, I., Karl, D., Spitzer, A., Gurlo, A., Günster, J., & Zocca, A. (2021). Characterisation of powder
460 flow behavior for additive manufacturing. *Additive manufacturing*, 47, 102250.
- 461 Cun, D., Zhang, C., Bera, H., & Yang, M. (2021). Particle engineering principles and technologies for
462 pharmaceutical biologics. *Advanced Drug Delivery Reviews*, 174, 140-167.
- 463 Deng, T., Garg, V., & Bradley, M. S. (2021). A study of particle adhesion for cohesive powders using a
464 novel mechanical surface energy tester. *Powder Technology*, 391, 46-56.
- 465 Deng, T., Garg, V., Diaz, L. P., Markl, D., Brown, C., Florence, A., & Bradley, M. S. (2022). Comparative
466 studies of powder flow predictions using milligrams of powder for identifying powder flow issues.
467 *International journal of pharmaceutics*, 628, 122309.
- 468 Deng, T., Garg, V., & Bradley, M. S. (2023). Electrostatic charging of fine powders and assessment of
469 charge polarity using an inductive charge sensor. *Nanomanufacturing*, 3(3), 281-292.
- 470 Donald, D. K. (1969). Electrostatic contribution to powder - particle adhesion. *Journal of Applied*
471 *Physics*, 40(7), 3013-3019.
- 472 Feng, J. Q., & Hays, D. A. (2003). Relative importance of electrostatic forces on powder particles.
473 *Powder Technology*, 135, 65-75.

474 Garg, V., Deng, T., & Bradley, M. S. (2022). A new method for assessing powder flowability based on
475 physical properties and cohesiveness of particles using a small quantity of samples. *Powder*
476 *Technology*, 395, 708-719.

477 Garg, V., Mallick, S. S., García-Trinanes, P., & Berry, R. J. (2018). An investigation into the flowability of
478 fine powders used in pharmaceutical industries. *Powder technology*, 336, 375-382.

479 Geldart, D., Abdullah, E. C., Hassanpour, A., Nwoke, L. C., & Wouters, I. J. C. P. (2006). Characterisation
480 of powder flowability using measurement of angle of repose. *China Particuology*, 4(3-4), 104-107.

481 Hays, D. A. (1995). Adhesion of charged particles. *Journal of adhesion science and technology*, 9(8),
482 1063-1073.

483 Hussain, T., Kaialy, W., Deng, T., Bradley, M. S., Nokhodchi, A., & Armour-Chélu, D. (2013). A novel
484 sensing technique for measurement of magnitude and polarity of electrostatic charge distribution
485 across individual particles. *International journal of pharmaceutics*, 441(1-2), 781-789.

486 Jenike, A. W. (1967). Denting of circular bins with eccentric drawpoints. *Journal of the Structural*
487 *Division*, 93(1), 27-35.

488 Johanson, K. (2012). Comparison of New Bulk Strength Measurement Technique with Traditional
489 Schulze (direct shear measurements) Method. Material Flow Solutions, Inc. USA

490 Karner, S., & Urbanetz, N. A. (2011). The impact of electrostatic charge in pharmaceutical powders
491 with specific focus on inhalation-powders. *Journal of Aerosol Science*, 42(6), 428-445.

492 Krantz, M., Zhang, H., & Zhu, J. (2009). Characterisation of powder flow: Static and dynamic testing.
493 *Powder Technology*, 194(3), 239-245.

494 Lefebvre, L. P., Pelletier, R., & Charbonneau, C. (2021). ELECTROSTATIC CHARGING AND ITS IMPACT
495 ON POWDER FLOWABILITY. *International Journal of Powder Metallurgy*, 57(4).

496 Liu, Z., Muzzio, F. J., & Callegari, G. (2023). Powder property change after passing through a feeder:
497 The effect of electrostatics on powder flow. *Powder Technology*, 425, 118532.

498 Mittal, K. L., & Jaiswal, R. (2015). Particle adhesion and removal. John Wiley & Sons.

499 Mizes, H., Ott, M., Eklund, E., & Hays, D. (2000). Small particle adhesion: measurement and control.
500 *Colloids and Surfaces A: Physicochemical and Engineering Aspects*, 165(1-3), 11-23.

501 Mullins, M. E., Michaels, L. P., Menon, V., Locke, B., & Ranade, M. B. (1992). Effect of geometry on
502 particle adhesion. *Aerosol Science and Technology*, 17(2), 105-118.

503 Peleg, M., Mannheim, C. H., & Passy, N. (1973). Flow properties of some food powders. *Journal of*
504 *Food Science*, 38(6), 959-964.

505 Quintanilla, M.A.S., Valverde, J. M., & Castellanos, A. (2006). Adhesion force between fine particles
506 with controlled surface properties. *AIChE journal*, 52(5), 1715-1728.

507 Rescaglio, A., Schockmel, J., Vandewalle, N., & Lumay, G. (2017). Combined effect of moisture and
508 electrostatic charges on powder flow. In *EPJ Web of Conferences* (Vol. 140, p. 13009). EDP Sciences.

509 Salazar-Banda, G.R., Felicetti, M.A., Gonçalves, J.A.S., Coury, J.R., & Aguiar, M.L. (2007). Determination
510 of the adhesion force between particles and a flat surface, using the centrifuge technique. *Powder*
511 *technology*, 173(2), 107-117.

512 Shah, U.V., Karde, V., Ghoroi, C., & Heng, J.Y. (2017). Influence of particle properties on powder bulk
513 behaviour and processability. *International journal of pharmaceutics*, 518(1-2), 138-154.

- 514 Suhag, R., Kellil, A., & Razem, M. (2024). Factors Influencing Food Powder Flowability. *Powders* 2024
515 (3): 65–76. doi.org/10.3390/powders3010006
- 516 Techaumnat, B., & Takuma, T. (2009). Analysis of the electrostatic force on a dielectric particle with
517 partial charge distribution. *Journal of Electrostatics*, 67(4), 686-690.
- 518 Tomas, J. (2000). Particle adhesion fundamentals and bulk powder consolidation. *KONA Powder and*
519 *Particle Journal*, 18, 157-169.
- 520 Zhou, H., Götzinger, M., & Peukert, W. (2003). The influence of particle charge and roughness on
521 particle–substrate adhesion. *Powder Technology*, 135, 82-91.